Electron energy loss in multilayered slabs. I. Normal incidence

1995 J. Phys.: Condens. Matter 7 3373

(http://iopscience.iop.org/0953-8984/7/18/003)

J. Phys.: Condens. Matter 7 (1995) 3373–3387. Printed in the UK

Electron energy loss in multilayered slabs: I. Normal incidence

J P R Bolton and M Chen

Physics Department, The Open University, Walton Hall, Milton Keynes MK7 6AA, UK

Received 28 July 1994, in final form 1 March 1995

Abstract. This work develops the semiclassical dielectric theory of energy loss, including retardation effects, for electrons travelling normal to a stratified slab. Starting from a transfer matrix formulation and using computer algebra, we obtain closed formulae for the dispersion relation, the Hertz vector and the energy-loss spectrum, valid for any finite number of layers. Our results are applied to multilayers of Al/Al_2O_3 and are used to investigate the validity of modelling a single interface by a sharp discontinuity in the dielectric function.

1. Introduction

Dielectric theory has been widely used to analyse energy-loss spectra obtained by scanning transmission electron microscopy. For example, a well-known semiclassical theory [1, 2] relates the energy-loss spectrum in a bulk medium to the imaginary part of the inverse of the dielectric function. The surface effects of a single homogeneous isotropic slab have also been thoroughly investigated. Otto and Kloos calculated the retarded dispersion relation for a single slab [3, 4]. The energy-loss spectrum for normal incidence on a single slab was calculated in the electrostatic limit by Ritchie [5] and in the retarded case by Kröger [6], who subsequently extended his calculation to cover oblique incidence on a single slab [7]. The case of parallel incidence has also been studied. Howie and co-workers [8, 9, 10] calculated the retarded energy-loss spectrum near a single interface and Parker performed a similar calculation for a beam passing parallel to a single homogeneous isotropic slab [11, 12].

This paper is the first part of a systematic investigation which extends the work cited above by deriving formulae, analogous to those of Kröger or Parker, but valid for multilayered and anisotropic slabs. The present paper gives the theory of normal incidence on multilayered slabs in which each layer is composed of a homogeneous isotropic medium. Subsequent papers will deal with parallel and oblique incidence on multilayered slabs and with slabs composed of anisotropic media. A general feature of this work is that it involves algebra of tedious length; this difficulty has been addressed by using computer algebra (REDUCE and MATHEMATICA) [13]. Our initial aim was to exploit computer algebra to derive answers in a few special cases (double- or triple-layered slabs, for example) but we have found that a *combination* of computer algebra and inductive argument produces more general results, valid for any number of layers.

The paper is organized as follows. Section 2 defines the problem and casts the boundary conditions in the form of a transfer matrix recurrence relation for the Hertz vector. This section does not advance beyond the work of Chase and Kliewer [14] but is included in order

0953-8984/95/183373+15$19.50

to establish important notation that is required later†. Section 3 introduces the concept of a dispersion bracket. Section 4 uses dispersion brackets to interpret the dispersion relation. In section 5, the transfer matrix recurrence relation is solved and general formulae obtained for the Hertz vector and the energy-loss function. Section 6 discusses the symmetries of these solutions and looks at some special cases. The theory is illustrated by numerical examples in section 7. We consider multilayered slabs of Al/Al_2O_3 and also use our formalism to examine whether it is reasonable to model a single interface by a sharp discontinuity in the dielectric function. The paper concludes with a summary in section 8.

Available space prevents us from reproducing all the steps in our analysis. We can only give an outline here, concentrating on our notation, general methods and final results. For readers who would like to follow the proofs in detail, we have prepared a lengthy internal report [15] which covers normal incidence, parallel incidence and anisotropic slabs. On the other hand, readers interested in our final results, rather than the techniques used to derive them, may wish to concentrate on equations (15), (17), (18) and (20) for general multilayered slabs and equations (23) and (24) for symmetric multilayered slabs. Note, however, that all these formulae are based on the concept of a dispersion bracket which is introduced and explained in section 3.

2. The transfer matrix recurrence relation

Consider a beam of particles, each of charge Q, travelling at constant speed v along the z-axis (figure 1). The beam passes through a multilayered slab of total thickness a which is stratified in the x–y-plane. The slab contains n layers (labelled $1, \ldots, n$) which extend infinitely in the x- and y-directions but are finite in the z-direction. The jth layer of the slab extends from z_{j-1} to z_j, has thickness $a_j = z_j - z_{j-1}$ and local dielectric function $\epsilon_j(\omega)$. The external regions (labelled 0 and $n+1$) extend from $z_{-1} = -\infty$ to $z_0 = 0$ and from $z_n = a$ to $z_{n+1} = \infty$; they are vacua, so $\epsilon_0 = \epsilon_{n+1} = 1$.

To apply the semiclassical dielectric formalism we must first solve Maxwell's equations. It is convenient to express all fields in terms of the Hertz vector [16] and to Fourier transform from (x, y, z, t) to (k_x, k_y, z, ω). In any given region, j, Maxwell's equations then reduce to a simple wave equation for the Fourier-transformed Hertz vector:

$$\left(\frac{\mathrm{d}^2}{\mathrm{d}z^2} - q_j^2\right) \boldsymbol{\Pi}^{(j)}(k_x, k_y, z, \omega) = \frac{Q\mathrm{e}^{\mathrm{i}\omega z/v}\hat{\boldsymbol{z}}}{\mathrm{i}\omega\epsilon_j\varepsilon_0} \tag{1}$$

where‡

$$q_j = \sqrt{k^2 - \epsilon_j\omega^2/c^2} \qquad \text{and} \qquad k = \sqrt{k_x^2 + k_y^2}.$$

Equation (1) is satisfied by taking

$$\Pi_x^{(j)} = \Pi_y^{(j)} = 0 \qquad \Pi_z^{(j)} = \left(\sum_{\sigma=\pm} A_j^\sigma e^{\sigma q_j z}\right) - \frac{Q\mathrm{e}^{\mathrm{i}\omega z/v}}{\mathrm{i}\omega\varepsilon_0}\frac{1}{\epsilon_j p_j^2} \tag{2}$$

where the symbol σ is used to denote $\pm$ (with $\sigma^2 = +$) and

$$p_j = \sqrt{k^2 - \epsilon_j\omega^2/c^2 + \omega^2/v^2}.$$

† [14] uses electric fields while our work is expressed in terms of the Hertz vector, but this difference is immaterial; more significantly, [14] provides only a numerical algorithm, while our work leads to closed-form solutions.

‡ Here and elsewhere, the square-root sign is taken to yield a quantity with a positive real part.

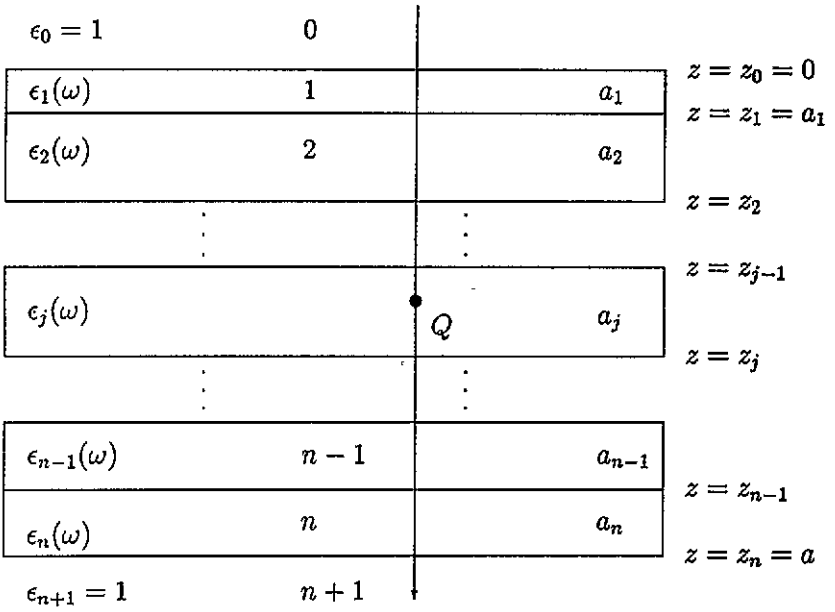

Figure 1. Multilayer geometry for normal incidence.

The $2n + 4$ coefficients A_j^σ must be determined from the boundary conditions. Because of axial symmetry, these coefficients depend only on k and ω. In principle, they can be found by allowing the Hertz vector to vanish at infinity and by solving the $2n+2$ linear equations obtained by requiring $\epsilon\Pi_z$ and $\partial\Pi_z/\partial z$ to be continuous at each interface (conditions that guarantee continuity of the transverse components of $\boldsymbol{E}$ and $\boldsymbol{H}$). In practice, this direct approach becomes unwieldy for slabs of more than three layers and it is better to incorporate the boundary conditions one interface at a time, using a transfer matrix recurrence relation to relate the Hertz vector coefficients in region j to those in region $j + 1$. In order to express this recurrence relation in the simplest possible form we first introduce *re-scaled* Hertz vector coefficients

$$\begin{aligned} \alpha_j^\sigma &= \frac{\varepsilon_0 v}{Q} A_j^\sigma \mathrm{e}^{(\sigma q_j - \mathrm{i}\omega/v)z_{j-1}} \qquad \text{for } j \geqslant 1 \\ \alpha_0^\sigma &= \frac{\varepsilon_0 v}{Q} A_0^\sigma \end{aligned} \tag{3}$$

and define the **coefficient vector** for region j:

$$\alpha_j = \begin{pmatrix} \alpha_j^+ \\ \alpha_j^- \end{pmatrix}.$$

Next, we introduce the variables

$$h_{ij}^\sigma = q_i\epsilon_j + \sigma q_j \epsilon_i \tag{4}$$

$$f_j = \mathrm{e}^{q_j a_j} \qquad \text{with } f_0 = f_{n+1} = 1 \tag{5}$$

$$b_j^\sigma = \mathrm{e}^{\sigma \mathrm{i}\omega a_j/v} \qquad \text{with } b_0^\sigma = b_{n+1}^\sigma = 1 \tag{6}$$

and define the **transfer matrix** from region j to region $j + 1$:

$$T^{(j+1,j)} = \begin{pmatrix} h_{j+1,j}^+ f_j^2 & h_{j+1,j}^- \\ h_{j+1,j}^- f_j^2 & h_{j+1,j}^+ \end{pmatrix}. \tag{7}$$

Finally, we introduce the variables

$$S_{ij}^{\sigma} = \frac{(\epsilon_i - \epsilon_j)s_{ij}^{\sigma}}{\epsilon_i p_i^2 p_j^2} \tag{8}$$

where

$$s_{ij}^{\sigma} = p_{ij}^2 + \sigma i \epsilon_i q_j v\omega/c^2$$

and

$$p_{ij} = \sqrt{k^2 - (\epsilon_i + \epsilon_j)\omega^2/c^2 + \omega^2/v^2}$$

and define the **source vector** for region j:

$$S_j = \begin{pmatrix} S_{j,j+1}^{+} \\ -S_{j,j+1}^{-} \end{pmatrix}. \tag{9}$$

The required recurrence relation, linking the Hertz vector coefficients in region j to those in region $j+1$, then takes the form

$$\boxed{h_{j+1,j+1}^{+}\alpha_{j+1} = \frac{1}{f_j b_j^{+}}\tau^{(j+1,j)}\alpha_j + S_j.} \tag{10}$$

This equation, which has been checked by REDUCE, summarizes the effect of the boundary conditions at the $(j+1)$th interface. Repeated application of this recurrence relation from $j = 0$ to $j = n$ allows us to link the coefficient vectors in the two external regions; the boundary conditions at $z = \pm\infty$ then give an expression for the coefficient vector in region 0:

$$\alpha_0^{+} = \frac{-1}{\tau_{11}^{(n+1,0)}} \sum_{k=0}^{n} \psi_{1k}^{+} \left(\tau_{11}^{(n+1,k+1)} S_{k,k+1}^{+} - \tau_{12}^{(n+1,k+1)} S_{k,k+1}^{-} \right) \qquad \alpha_0^{-} = 0 \tag{11}$$

where

$$\psi_{ij}^{\sigma} = \prod_{k=i}^{j} h_{kk}^{+} f_k b_k^{\sigma} \qquad \text{with initial value } \psi_{i,i-1}^{\sigma} = 1$$

and

$$\tau^{(ji)} = \prod_{k=i}^{j-1} \tau^{(k+1,k)} \qquad \text{(with the product ordered from right to left).} \tag{12}$$

The dispersion relation for an n-layered slab follows immediately:

$$\tau_{11}^{(n+1,0)} = 0. \tag{13}$$

Moreover, once the coefficient vector is known in region 0, equation (10) can be used to find the coefficient vectors in all the other regions. In principle, the electric field acting on the electron and the total energy loss can then be calculated algebraically. Unfortunately, a straightforward application of this procedure generates coefficient vectors that become increasingly complicated as one progresses through the multilayered slab, and the resulting expression for the energy loss is very complicated indeed, even for double or triple slabs. It is always possible to proceed numerically [13, 14, 17], but this approach provides no insight into the analytic form of the solution or its relationship to the well-known results established for a single slab [6, 7].

Since the main aim of this work is to provide closed formulae for the dispersion relation and the energy loss probability, valid for any number of layers and expressed in the simplest

possible terms, a different approach is needed. Simplicity is essential but elusive; without special care, the results obtained are of paralysing complexity. A natural response to this complexity is to use computer algebra and we have applied both REDUCE and MATHEMATICA to simplify the solutions for low values of n. This process is by no means automatic and we have supplemented the standard programs with packages of our own which facilitate the simplification of large multinomials. In this way, we obtain solutions that are simplified as far as possible for $n = 1$, 2 and 3. These solutions follow a definite pattern, allowing us to guess the general form of solutions for arbitrary n. The final stage of our analysis is to use mathematical induction to prove that these tentative guesses are correct. The role of computer algebra is therefore heuristic; we would have found it difficult to construct our final solutions without using computer algebra, yet our final proofs do not rely on it.

3. The dispersion bracket formalism

Our formulae for the dispersion relation and the energy loss are best expressed in terms of a new algebraic operation which is defined for any product of terms bearing $\pm$ superscripts interspersed by f^2-factors, such as $h^-_{32}f^2_2h^+_{21}f^2_1h^-_{10}$. The product is assumed to be ordered so that the subscripts increase monotonically from one end to the other. We then define a **contraction** of the ordered product by choosing two terms with $\pm$ superscripts, reversing the signs of these superscripts and removing all the f^2-factors between them. The contraction is represented by a square overbrace so, for example,

$$\overbrace{h^-_{32}f^2_2h^+_{21}f^2_1h^-_{10}} = h^-_{32}f^2_2h^-_{21}h^+_{10}.$$

We invariably need to consider the *sum* of all *non-overlapping* contractions of the ordered product, including the term with no contractions. Such a sum will be referred to as a **dispersion bracket** and denoted by enclosing the product in *square* brackets. For example,

$$\begin{aligned}&\left[h^-_{32}f^2_2h^+_{21}f^2_1h^-_{10}\right]\\ &= h^-_{32}f^2_2h^+_{21}f^2_1h^-_{10} + \overbrace{h^-_{32}f^2_2h^+_{21}}f^2_1h^-_{10} + \overbrace{h^-_{32}f^2_2h^+_{21}f^2_1h^-_{10}} + h^-_{32}\overbrace{f^2_2h^+_{21}f^2_1h^-_{10}}\\ &= h^-_{32}f^2_2h^+_{21}f^2_1h^-_{10} + h^+_{32}h^-_{21}f^2_1h^-_{10} + h^+_{32}h^+_{21}h^+_{10} + h^-_{32}f^2_2h^-_{21}h^+_{10}.\end{aligned}$$

In general, a product containing n-factors with $\pm$ superscripts yields a dispersion bracket which is the sum of 2^{n-1} terms. The dispersion brackets of several different products will be used in this work. The fundamental product is

$$C_{ji} = \prod_{k=i}^{j} h^+_{k+1,k}f^2_k = \prod_{k=i}^{j} f^2_k h^+_{k,k+1} \qquad \text{for } j \geqslant i$$

with $C_{i-1,i} = 1$ and $C_{i-2,i} = 0$. Other products can then be defined in terms of C_{ji}:

$$\begin{aligned}D_{ji} &= C_{j,i+1}h^-_{i+1,i}\\ E_{ji} &= h^-_{j+1,j}f^2_jC_{j-1,i}\\ F_{ji} &= h^-_{j+1,j}f^2_jC_{j-1,i+1}h^-_{i+1,i} \qquad \text{for } j \geqslant i+1\end{aligned}$$

with $F_{ii} = h^+_{i+1,i}$, $F_{i-1,i} = 1$ and $F_{i-2,i} = 0$. Dispersion brackets of these products arise naturally in our analysis because

$$\tau^{(j+1,i)} = \begin{pmatrix}\left[C_{ji}\right] & \left[D_{ji}\right]\\ \left[E_{ji}\right] & \left[F_{ji}\right]\end{pmatrix}. \tag{14}$$

This result was first checked by computer algebra for $j - i \leqslant 10$ and then proved by mathematical induction for arbitrary $j - i$ [15, 18]. It provides an alternative method for evaluating the matrix elements of $\tau^{(ji)}$. Rather than using the direct matrix multiplication of (12) we can use the dispersion bracket expansion outlined above, the latter approach being especially convenient for low-order products ($j - i \leqslant 5$ or so). Moreover, the importance of dispersion brackets extends beyond the matrix elements of the $\tau^{(ji)}$. In section 5, we shall use the dispersion brackets of two further products:

$$X^{\sigma}_{ji} = S_{j+1,j} f_j^2 C_{j-1,i}$$

$$Y^{\sigma}_{ij} = S^{\sigma}_{i,i+1} C_{j,i+1}.$$

Introduction of these quantities allows us to develop algebraic methods, valid for slabs containing any number of layers, which eventually yield a compact formula for the energy-loss probability. For ease of reference, we summarize our definitions in table 1, using a more explicit notation. With these definitions in place, we are in a good position to describe our main results.

C_{ji}	=	$h^+_{j+1,j} f_j^2 \ldots h^+_{i+1,i} f_i^2$	with	C_{ii}	=	$h^+_{i+1,i} f_i^2$	and	$C_{i,i+1} = 1$
D_{ji}	=	$h^+_{j+1,j} f_j^2 \ldots h^-_{i+1,i}$	with	D_{ii}	=	$h^-_{i+1,i}$	and	$D_{i,i+1} = 0$
E_{ji}	=	$h^-_{j+1,j} f_j^2 \ldots h^+_{i+1,i} f_i^2$	with	E_{ii}	=	$h^-_{i+1,i} f_i^2$	and	$E_{i,i+1} = 0$
F_{ji}	=	$h^-_{j+1,j} f_j^2 \ldots h^-_{i+1,i} f_i^2$	with	F_{ii}	=	$h^+_{i+1,i}$	and	$F_{i,i+1} = 1$
X^{σ}_{ji}	=	$S^{\sigma}_{j+1,j} f_j^2 \ldots h^+_{i+1,i} f_i^2$	with	X^{σ}_{ii}	=	$S^{\sigma}_{i+1,i} f_i^2$	and	$X^{\sigma}_{i,i+1} = 0$
Y^{σ}_{ij}	=	$S^{\sigma}_{i,i+1} f_{i+1}^2 \ldots h^+_{j,j+1}$	with	Y^{σ}_{ii}	=	$S^{\sigma}_{i,i+1}$	and	$Y^{\sigma}_{i+1,i} = 0$

Table 1. Products needed in dispersion brackets.

4. The dispersion relation

The concept of a dispersion bracket has an immediate application in interpreting (13). Using equations (14) and (5), the dispersion relation for an n-layered slab becomes

$$\boxed{[C_{n0}] = [h^+_{n+1,n} f_n^2 \ldots h^+_{10}] = 0.} \tag{15}$$

This result agrees with all known results for low n. For example, setting $n = 1$ gives

$$0 = [C_{10}] = h^+_{21} f_1^2 h^+_{10} + h^-_{21} h^-_{10} = (h^+_{10})^2 f_1^2 - (h^-_{10})^2$$

in agreement with [19]. The results of [17] for double† and triple slabs are obtained by setting $n = 2$ and $n = 3$ in (15) and taking the electrostatic limit. Elsewhere ([15] and [20]), we have also examined our results in the limit of a superlattice with a arbitrary basis unit, and have verified that (15) reproduces the results of a calculation that directly applies Bloch's theorem to a periodic structure.

† It is necessary to correct an obvious misprint in Richter and Geiger's expression for a double slab.

5. The Hertz vector and energy loss

In order to obtain an expression for the electron energy-loss spectrum we must first calculate the Hertz vector in each region inside and outside the slab. Our computer algebra programs suggest the following general formula for the coefficient vector in the jth region of an n-layer slab:

$$\alpha_j = \frac{1}{[C_{n0}]}\left\{\sum_{k=0}^{j-1}\psi^-_{k+1,j-1}\left[X^-_{k0}\right]M_{nj} - f_j b_j^+ \sum_{k=j}^{n}\psi^+_{j+1,k}\left[Y^+_{kn}\right]N_{j-1,0}\right\} \quad (16)$$

where

$$M_{ji} = \begin{pmatrix} -\left[D_{ji}\right] \\ \left[C_{ji}\right] \end{pmatrix} \qquad \text{and} \qquad N_{ji} = \begin{pmatrix} \left[C_{ji}\right] \\ \left[E_{ji}\right] \end{pmatrix}.$$

This result was first checked by computer algebra for $n \leqslant 7$ and then proved by mathematical induction for arbitrary n. In other words, we have shown that our previous expression for α_0^σ (equation (11)) is recovered on substituting $j = 0$ in (16) and then confirmed that the transfer matrix recurrence relation (equation (10)) guarantees that, if (16) is valid for $j = i$, then it is also valid for $j = i + 1$. The interested reader is referred to [15] and [18] for full details.

Equation (16) is not of primary interest in the present study, but it is a vital step towards finding the energy-loss spectrum. By calculating the work done on the incoming particle by the electric field induced in the slab, and interpreting the result in terms of the transfer of quanta of energy $\hbar\omega$, we can find the semiclassical energy loss function $\mathrm{d}^2P/\mathrm{d}(\hbar\omega)\,\mathrm{d}k$. This is normalized in such a way that the work done by a particle traversing the multilayered slab is given by

$$W = 2\pi\int_0^\infty \mathrm{d}(\hbar\omega)\,\hbar\omega\int_0^\infty \mathrm{d}k\,k\frac{\mathrm{d}^2P}{\mathrm{d}(\hbar\omega)\,\mathrm{d}k}.$$

The energy-loss function can then be expressed as

$$\frac{\mathrm{d}^2P}{\mathrm{d}(\hbar\omega)\,\mathrm{d}k} = \frac{Q^2}{4\pi^3\varepsilon_0\hbar^2v^2}\mathrm{Im}\left(\chi_{\mathrm{bulk}} + \chi_{\mathrm{bdy}}\right) \quad (17)$$

where χ_{bulk} represents the bulk contribution and χ_{bdy} represents the boundary contributions (due to surfaces and interfaces). Our calculation shows that the bulk contribution is a sum over layers, with the ith layer contributing an amount equal to its thickness times the energy loss per unit length in an infinite sample of the ith medium [2]:

$$\boxed{\chi_{\mathrm{bulk}} = \sum_{i=1}^{n}\frac{a_i}{p_i^2}\left(\frac{v^2}{c^2} - \frac{1}{\epsilon_i}\right).} \quad (18)$$

The boundary contributions are more complicated. They are formally given by

$$\chi_{\mathrm{bdy}} = \sum_{i=0}^{n+1}\frac{k^2}{p_i^2}\sum_{\sigma=\pm}(1 - \sigma\mathrm{i}q_iv/\omega)\,\alpha_i^\sigma c_i^\sigma$$

where

$$c_i^\sigma = \begin{cases} 1 & \text{if } i = 0 \\ f_i^\sigma b_i^- - 1 & \text{if } 1 \leqslant i \leqslant n \\ -1 & \text{if } i = n+1. \end{cases}$$

These expressions, combined with (16), yield a very lengthy expression for the energy-loss spectrum. Our main algebraic task has been to reduce this expression to a manageable form. After a considerable amount of algebra [18, 15], the boundary contribution to the energy-loss function emerges as a sum of *factored* terms:

$$\boxed{\chi_{\text{bdy}} = -\frac{k^2}{[C_{n0}]} \sum_{i=0}^{n} \sum_{j=i}^{n} \sum_{\sigma=\pm} z_{ij} \psi^{\sigma}_{i+1,j} \left[X^{\sigma}_{i0}\right] \left[Y^{\sigma}_{jn}\right]} \tag{19}$$

where

$$z_{ij} = \begin{cases} \frac{1}{2} & \text{if } i = j \\ 1 & \text{otherwise.} \end{cases}$$

An alternative, somewhat more explicit, form is

$$\boxed{\chi_{\text{bdy}} = \frac{k^2}{[C_{n0}]} \sum_{i=0}^{n} \sum_{j=i}^{n} \frac{(\epsilon_i - \epsilon_{i+1})(\epsilon_j - \epsilon_{j+1})}{\epsilon_{i+1}\,\epsilon_j\; p_i^2\, p_{i+1}^2\; p_j^2\, p_{j+1}^2}\, T^{(n)}_{ij}} \tag{20}$$

where

$$T^{(n)}_{ij} = \sum_{\sigma=\pm} z_{ij}\, \psi^{\sigma}_{i+1,j} \left[x^{\sigma}_{i0}\right] \left[y^{\sigma}_{jn}\right] \tag{21}$$

and x^{σ} and y^{σ} are relatives of X^{σ} and Y^{σ}, obtained by replacing S^{σ} by s^{σ}.

Equations (18) and (20) are the main theoretical results of this paper. They provide a remarkably simple expression for the semiclassical energy-loss spectrum, valid for normal incidence on an arbitrary multilayered slab. In the special case $n = 1$, these equations reduce to

$$\chi_{\text{bulk}} + \chi_{\text{bdy}} = \frac{a}{p_1^2}\left(\frac{v^2}{c^2} - \frac{1}{\epsilon_1}\right) + \frac{k^2(\epsilon_1 - \epsilon_0)^2}{\epsilon_1 \left[C_{10}\right] p_0^4 p_1^4} \sum_{\sigma=\pm} s^{\sigma}_{10} \left(\frac{1}{\epsilon_0}\left[x^{\sigma}_{10}\right] - \frac{\psi^{\sigma}_{11}}{\epsilon_1} s^{\sigma}_{10}\right)$$

which is a compact form of Kröger's expression for normal incidence on a single slab [6]. This type of checking cannot be pressed further because there are no published formulae for $n > 1$, however we have checked that (19) agrees with the solution for $n = 2$ which we obtained using the direct approach mentioned just below (2) in section 2. Further checks based on symmetry properties are presented in the next section.

6. Symmetries and symmetrical slabs

Having constructed closed-form solutions for the dispersion relation, the Hertz vector and the energy-loss function, we now investigate their symmetry properties and examine the simplifications that arise for symmetrical slabs. We define five operators:

(i) $\hat{\mathcal{P}}_k$ reverses the sign of q_k but leaves q_j unchanged for $j \neq k$;

(ii) $\hat{\mathcal{S}}$ reverses the labelling of the regions so that $k \to n + 1 - k$;

(iii) $\hat{\mathcal{T}}_v$ reverses the sign of v;

(iv) $\hat{\mathcal{T}}_\omega$ reverses the sign of ω;

(v) $\hat{\mathcal{J}}_{k,k+1}$ causes two neighbouring regions k and $k + 1$ to coalesce (accomplished by setting $\epsilon_{k+1} \to \epsilon_k$, $q_{k+1} \to q_k$ etc, $2a_k \to a_k$ and then renumbering $j \to j - 1$ for $j \geqslant k$).

6.1. The dispersion relation

It is easy to see that $[C_{n0}]$ is invariant under $\hat{S}$ and $\hat{T}_v$. We have also proved [18] that

$$\hat{\mathcal{P}}_k([C_{n0}]) = -[C_{n0}]/f_k^2 \qquad \text{for } k = 1, \ldots, n \tag{22}$$

and

$$\hat{T}_\omega([C_{n0}]) = [C_{n0}]^* .$$

It follows that the dispersion relation ((15)) is invariant under all four symmetry operations, as it must be. Moreover,

$$\hat{\mathcal{J}}_{k,k+1}([C_{n0}]) = h_{kk}^+ [C_{n-1,0}]$$

so the dispersion relation correctly becomes that for an $(n-1)$-layered slab when two neighbouring regions coalesce.

6.2. The Hertz vector

The Hertz vector coefficients, calculated from (16), obey the identities

$$\hat{\mathcal{P}}_k(\alpha_j^\sigma) = \begin{cases} \alpha_j^{-\sigma} & \text{if } k = j \\ \alpha_j^\sigma & \text{if } k \neq j \end{cases}$$

$$\hat{S}\hat{T}_v(\alpha_j^\sigma) = -\mathrm{e}^{-(\sigma q_{n+1-j} + \mathrm{i}\omega/v)a_{n+1-j}} \alpha_{n+1-j}^{-\sigma}.$$

These identities mean that the Hertz vector can be reconstructed from a partial knowledge of its coefficients†. For example, if the α_j^+ are known algebraic functions from $j = 0$ to $j = \text{Ceiling}(n/2)$, the remaining coefficients and hence the full Hertz vector can be found by applying the operators $\hat{\mathcal{P}}_k$ and $\hat{S}\hat{T}_v$. When two neighbouring regions coalesce the coefficients of the Hertz vector transform in the expected way. Using $\alpha_j^\sigma(m)$ to denote the coefficients for the jth layer in an m-layered slab, (16) gives

$$\hat{\mathcal{J}}_{k,k+1}(\alpha_j^\sigma(n)) = \alpha_j^\sigma(n-1) \qquad \text{for } 1 \leqslant j \leqslant k-1$$

$$\hat{\mathcal{J}}_{k,k+1}(\alpha_j^\sigma(n)) = \alpha_{j-1}^\sigma(n-1) \qquad \text{for } k+1 \leqslant j \leqslant n$$

as expected.

6.3. The energy-loss function

Finally, we can show that (19) provides an energy-loss function χ_{bdy} that is invariant under the symmetry operations $\hat{\mathcal{P}}_k$, $\hat{T}_v$ and $\hat{S}$ so the energy loss caused by a (possibly asymmetric) sample is predicted to be independent of the sense of travel of the beam. Also,

$$\hat{T}_\omega(\chi_{\text{bulk}}) = \chi_{\text{bulk}}^* \qquad \text{and} \qquad \hat{T}_\omega(\chi_{\text{bdy}}) = \chi_{\text{bdy}}^*$$

as expected. Moreover, (19) produces a result appropriate to $n-1$ layers when two neighbouring regions coalesce. We further note that

$$\hat{S}(T_{ij}^{(n)}) = T_{n-j,n-i}^{(n)}.$$

This identity can be used to simplify calculations based on (20): instead of evaluating $\frac{1}{2}(n+1)(n+2)$ different $T_{ij}^{(n)}$-terms, we can concentrate on (Floor$(n/2)+1$)(Ceiling$(n/2)+1$) terms, obtaining the remainder by means of the transformation $k \to n+1-k$.

† In the following discussion the term Ceiling(x) denotes the smallest integer that is greater or equal to x and Floor(x) denotes the greatest integer that is smaller or equal to x.

6.4. Symmetrical slabs

The symmetry properties discussed above lead to simplifications when the slab is symmetrical about its middle layer. We consider a slab containing $n = 2m+1$ layers, whose geometric and dielectric properties are symmetrical about the $(m+1)$th layer: $a_k = a_{2m+2-k}$ and $\epsilon_k = \epsilon_{2m+2-k}$. We have proved that the dispersion relation for such a slab can always be factored as follows:

$$\boxed{\left[C_{2m+1,0}\right] = L^{+}_{m0} L^{-}_{m0} = 0} \tag{23}$$

where

$$L^{\sigma}_{m0} = \left[C_{m0}\right] f_{m+1} + \sigma \left[E_{m0}\right].$$

This result agrees with the special cases $m = 0$, $m = 1$, $m = 2$ and $m = 3$ discussed in [19] and [21]. In general, the factorization of the dispersion relation is a considerable simplification. Its physical significance can be understood by noting that the solutions of $L^{\sigma}_{m0} = 0$ obey

$$\frac{A^{+}_{n+1-j} \mathrm{e}^{q_j a/2}}{A^{-}_{j} \mathrm{e}^{-q_j a/2}} = -\sigma.$$

This shows that the solutions of $L^{+}_{m0} = 0$ are antisymmetric in their Hertz vectors (and electric fields) and therefore symmetric in their charge distributions: these modes will be described as being *symmetric*. By a similar argument, the solutions of $L^{-}_{m0} = 0$ are antisymmetric in their charge distributions. In both cases, the modes have a TM character.

Another useful simplification occurs in the formula for the energy-loss spectrum. For a symmetrical slab the energy-loss function due to boundaries can be expressed as

$$\boxed{\chi_{\mathrm{bdy}} = \frac{2k^2}{L^{+}_{m0} L^{-}_{m0}} \sum_{i=0}^{m} \sum_{j=i}^{n-i} \frac{(\epsilon_i - \epsilon_{i+1})(\epsilon_j - \epsilon_{j+1})}{\epsilon_{i+1}\, \epsilon_j\, p_i^2\, p_{i+1}^2\, p_j^2\, p_{j+1}^2} t^{(n)}_{ij}} \tag{24}$$

where

$$t^{(n)}_{ij} = \sum_{\sigma=\pm} z_{ij} z_{i,n-j} \psi^{\sigma}_{i+1,j} \left[x^{\sigma}_{i0}\right] \left[y^{\sigma}_{jn}\right].$$

This result involves only $(m+2)/(2m+3)$ as many terms as (20) for a general $2m+1$ layer slab. Kröger's result for a single slab is regained on setting $m = 0$.

7. Applications of the energy loss formula

Our expression for the energy-loss function $\mathrm{d}^2P/\mathrm{d}(\hbar\omega)\,\mathrm{d}k$ can be integrated over transverse wavevectors to obtain the scattering probability per unit energy range, $I(\hbar\omega)$. If all the scattered electrons were collected, one would expect that

$$I(\hbar\omega) = 2\pi \int_0^{\infty} \mathrm{d}k\, k\, \frac{\mathrm{d}^2 P}{\mathrm{d}(\hbar\omega)\,\mathrm{d}k} = \frac{Q^2}{2\pi^2 \varepsilon_0 \hbar^2 v^2} \int_0^{\infty} \mathrm{d}k\, k\, \mathrm{Im}(\chi_{\mathrm{bulk}} + \chi_{\mathrm{bdy}}).$$

Unfortunately, as is always found in energy-loss problems, the bulk term produces a logarithmic divergence at large k. On the other hand, (20) shows that the terms due to surfaces and boundaries are well-behaved and produce no additional divergencies. The logarithmic divergence is dealt with as usual [22], by introducing an upper cut-off k_c. If all the scattered electrons were collected, $1/k_c$ would set a minimum length scale for the validity of our semiclassical continuum model. In practice, k_c is often determined by the sizes of

various apertures inside the electron microscope which restrict the scattering angle. In the following examples the beam energy has been set at 100 keV and the cut-off wavevector has been chosen to be 15 nm^{-1} (corresponding to scattering through a maximum angle of 9 mrad).

The expressions for χ_{bulk} and χ_{bdy} provide a framework for interpreting energy-loss spectra in multilayered slabs. Equation (18) yields bulk peaks in the energy-loss spectrum when $\epsilon_i \simeq 0$ (bulk longitudinal plasmon in ith layer) and when $p_i \simeq 0$ (Cherenkov radiation in ith layer). However, the intensities of these peaks may be significantly modified by boundary effects, as (20) shows that χ_{bdy} also has peaks at $\epsilon_i \simeq 0$ and $p_i \simeq 0$. It is natural to distinguish contributions to χ_{bdy} with $k < \omega/c$ (radiative modes) from those with $k > \omega/c$ (non-radiative modes).

The most interesting feature of (20) is that additional peaks appear when the dispersion relation is close to being satisfied ($[C_{n0}] \simeq 0$). Using (22) we can show that the dispersion relation is satisfied by taking $q_i = 0$ for any i between 1 and n. These solutions are independent of geometry and correspond to *transverse bulk modes* in the various layers of the slab. The remaining solutions of the dispersion relation correspond to true surface and interfacial modes. In all cases, (20) predicts a scattering probability that is proportional to products of differences of dielectric functions. The contribution of surface, interfacial and transverse modes will therefore be small if the materials involved have similar dielectric properties, as is the case for many semiconductors. Our numerical calculations confirm this fact. The best chance of observing interfacial modes arises if the materials have very different dielectric functions at frequencies for which $[C_{n0}]$ is close to zero (for typical values of k). This condition can often be met for metal–metal, metal–insulator and semiconductor–insulator interfaces.

To illustrate our equations, we take the case of Al/Al_2O_3 double and triple slabs. (Further applications, including metal–metal and MOS structures, are discussed in [13] and [23].) The dielectric function of bulk aluminium is taken to be

$$\epsilon(\omega) = 1 - \omega_p^2/(\omega^2 + i\omega\omega_0) \tag{25}$$

with $\hbar\omega_p = 15.0$ eV and $\hbar\omega_0 = 0.6$ eV and, for ease of comparison with [17], the dielectric function of Al_2O_3 is modelled by a constant, $\epsilon_{Al_2O_3} = 4$.

Figure 2 shows the calculated scattering probability per unit energy range for an Al/Al_2O_3 double slab, with each layer of thickness $d = 100$ Å. There are two sharp peaks located around 15 eV and 10.7 eV and a much broader peak which reaches its maximum value at 6.5 eV, but which spreads to lower energies. These peaks correspond to bulk Al, surface Al and Al/Al_2O_3 interfacial plasmons. There are no bulk or surface losses due to Al_2O_3, because the dielectric function of this material has been taken to be real and positive. Our interpretation is assisted by figure 3, which shows how $2\pi k\, d^2P/d(\hbar\omega)\, dk$ varies as a function of k and $\hbar\omega$. The three main ridges on this diagram correspond to the dispersion relations for bulk, surface and interface modes. Above 15 eV there are faint traces of a transverse bulk mode, but this does not contribute significantly to $I(\hbar\omega)$. In our model, the bulk mode shows no dispersion. The surface mode exhibits dispersion for $kd < 1$ but, because the scattering is dominated by the high-k region, the surface peak in $I(\hbar\omega)$ remains narrow. The interface mode is much broader because the high-k region no longer dominates. In terms of (20), the factors of p_i^2 and $[C_{n0}]$ in the denominator of χ_{bdy} can both be small at low k and low ω, giving rise to significant scattering from relatively small regions of k–ω-space.

A slightly more complicated situation arises when both surfaces of a central aluminium layer are coated by oxide. Figures 4 and 5 show $I(\hbar\omega)$ and $2\pi k\, d^2P/d(\hbar\omega)\, dk$ for a triple-

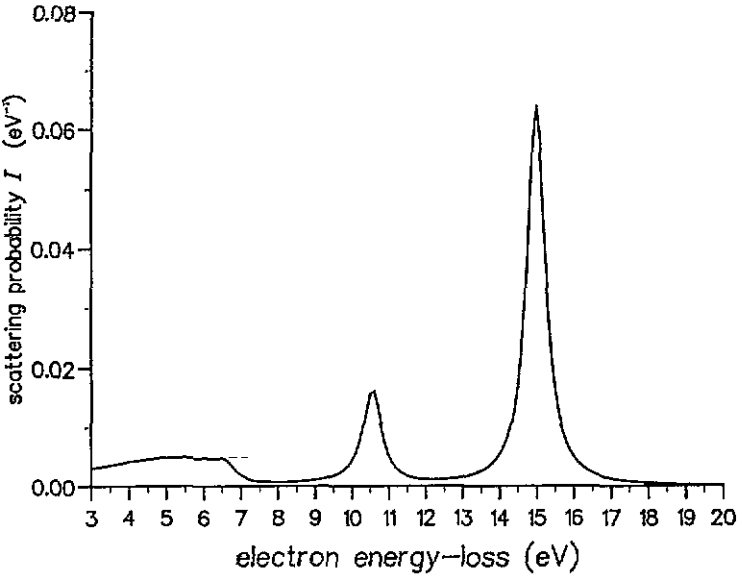

Figure 2. The scattering probability per unit energy range $I(\hbar\omega)$ for normal incidence on an Al/Al_2O_3 double layer. The thickness of each layer is $d = 100$ Å. For reasons explained in section 6.3, the sense of propagation through the slab is immaterial. The bulk Al, surface Al and Al/Al_2O_3 interface peaks are at 15 eV, 10.7 eV and at 6.5 eV and below.

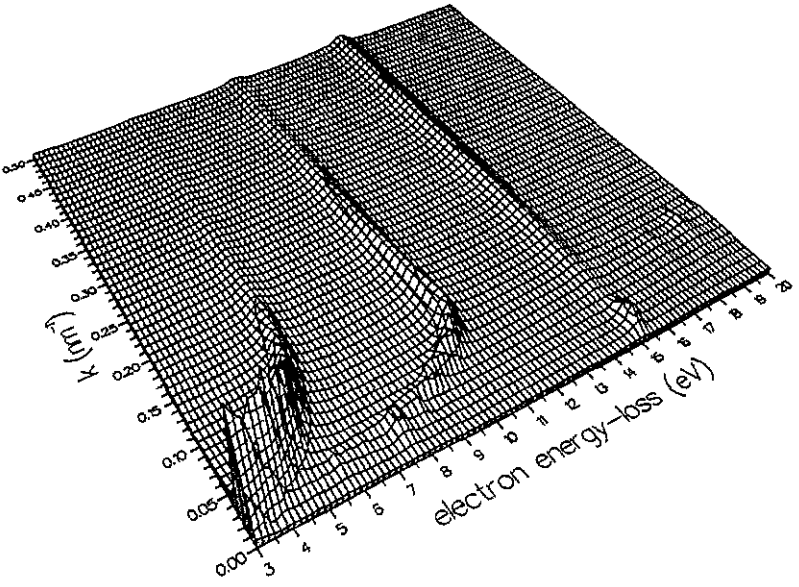

Figure 3. A three-dimensional plot of $2\pi k\, d^2P/d(\hbar\omega)\, dk$ against k and $\hbar\omega$ for normal incidence on the Al/Al_2O_3 double-layer system of figure 2. The three main ridges correspond to Al bulk, Al surface and interfacial plasmons. The surface and (more importantly) the interfacial plasmons are broadened towards lower frequencies as a result of scattering at low k.

layered $Al_2O_3/Al/Al_2O_3$ structure, with each layer of thickness 100 Å. This geometry ensures that there is no surface Al peak, but the peak due to interfacial plasmons now has a richer structure between 6 eV and 8 eV, because of coupling of modes at the two metal–

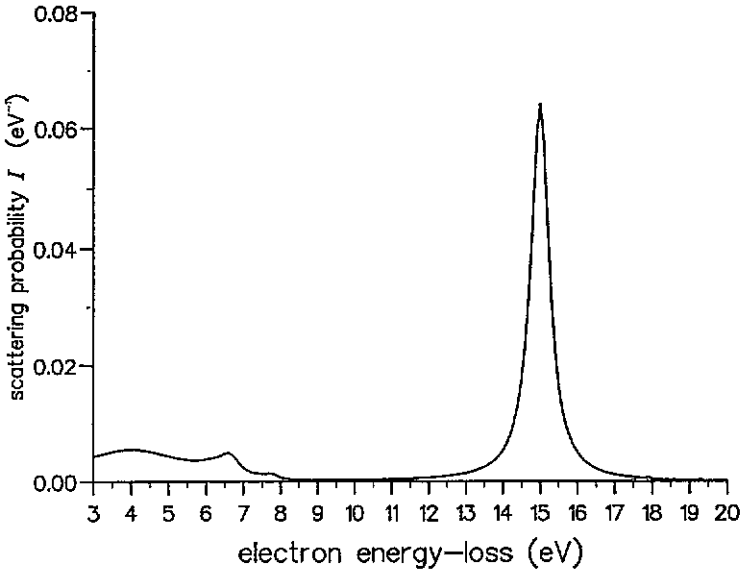

Figure 4. The scattering probability per unit energy range for normal incidence on a symmetric three-layer system $Al_2O_3/Al/Al_2O_3$. The thickness of each layer is taken to be 100 Å. The bulk Al peak is at 15 eV and the Al/Al_2O_3 interface modes are around 7 eV.

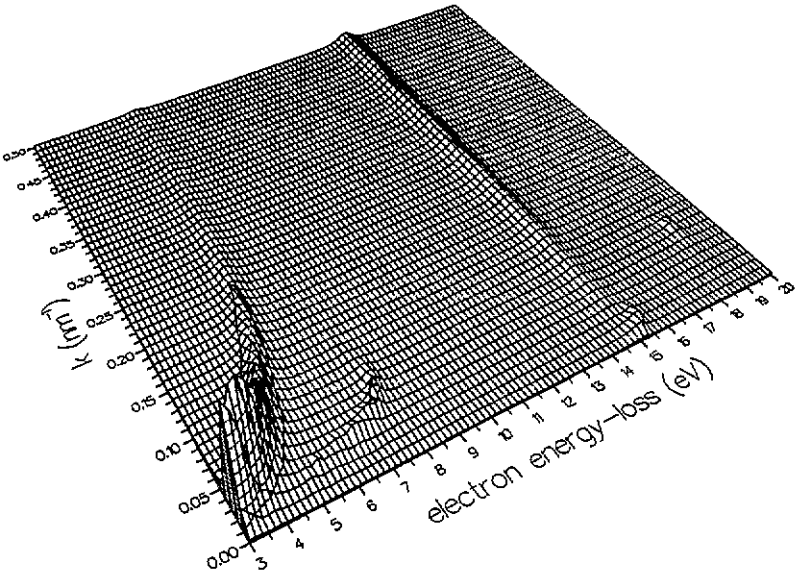

Figure 5. A three-dimensional plot of $2\pi k\, d^2P/d(\hbar\omega)\, dk$ against k and $\hbar\omega$ for normal incidence on the $Al_2O_3/Al/Al_2O_3$ system of figure 4. The three main ridges correspond to Al bulk plasmons, antisymmetric interfacial plasmons and symmetric interfacial plasmons.

oxide interfaces, leading to distinct symmetric and antisymmetric modes. The overall picture is similar to that described by Richter and Geiger [17], but the interface modes predicted by our retarded calculation are broader and less pronounced than those predicted in [17] (which is based on an electrostatic approximation).

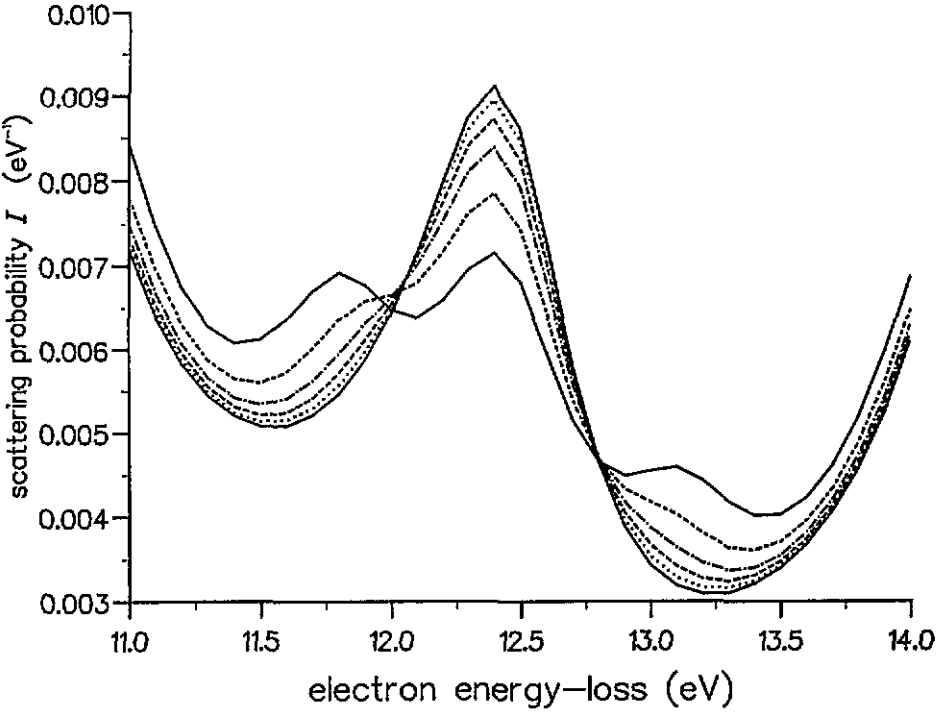

Figure 6. The scattering intensity for normal incidence on an Al/Mg bilayer in the region of the interfacial plasmon. Both layers are 100 Å thick. The dielectric function of Al is modelled by (25) as explained above, while that of Mg is taken to have a similar form but with $\hbar\omega_p = 10.0$ eV. In the interfacial region the dielectric properties are varied from those of bulk Al to those of bulk Mg in five equal steps. The abruptness of the transition is explored by varying the thickness τ of the individual steps. The highest peak corresponds to an infinitely sharp boundary ($\tau = 0$). The remaining peaks are for $\tau = 0.2$ Å, 1.0 Å, 2.0 Å, 3.0 Å and 5.0 Å, corresponding to total healing lengths of 1.0 Å, 5.0 Å, 10.0 Å, 15.0 Å and 25.0 Å.

Finally, we use our theory of multilayered slabs to investigate whether it is reasonable to model a *single* interface by a sharp discontinuity in the dielectric function. We imagine a *local* dielectric function that varies smoothly near the interface of two materials, healing over a characteristic length of a few Å. We may assume that the scattering due to this dielectric function is similar to that of a multilayered slab, formed by approximating the dielectric function by a series of step functions. We can then vary the thicknesses of the layers in the multilayered slab, mimicking the effect of smearing out the discontinuity at the interface. Figure 6 reveals the results of this procedure. It shows that the interfacial peak in the energy-loss spectrum is diminished by less than 30% if the dielectric function heals over a distance of 15 Å or less.

The local model used to construct figure 6 is rather artificial [24] but we believe that it illustrates a fact of some practical importance—the sensitivity of interfacial energy-loss peaks to the sharpness of the discontinuity at the interface. In many cases, the dielectric function will vary over just a few atomic layers so the model of a sharp discontinuity should remain a reasonable first approximation. In some cases, however, the discontinuity will take place more gradually and the interfacial peaks will be strongly suppressed. This may be the case at a Si/SiO_2 interface [25] and will also occur when one material diffuses into another. Indeed, it may be possible to calibrate this effect and to use the result to monitor the onset

of diffusion at an interface.

8. Summary

Equations (15) and (19) derived in this paper provide a straightforward way of calculating the retarded dispersion relation and retarded electron energy-loss spectrum for normal incidence on any multilayered slab. We have expressed these results in as simple a form as possible, examined their symmetry properties and checked them against all known results. Further simplifications have been obtained for symmetric slabs (equations (23) and (24)).

Energy-loss spectra obtained under conditions of normal incidence are predicted to contain peaks due to the excitation of coupled interface modes. These peaks are indistinct in common semiconductor–semiconductor structures, but are significant in many other cases. We have examined Al/Al_2O_3 double and triple slabs and obtained clear interfacial peaks, although these are less pronounced than suggested by a previous electrostatic calculation. Finally, we have shown that scattering at a single interface is likely to be overestimated in models that assume an abrupt transition from the bulk properties of one material to the bulk properties of another. At atomically sharp interfaces the overestimate should be modest, but in other cases it may be significant. It should be possible to use this effect to estimate the amount interfacial diffusion from the size of the interfacial plasmon peak.

References

[1] Fermi E 1940 *Phys. Rev.* **57** 485–493
[2] Landau L D and Lifshitz E M 1960 *Electrodynamics of Continuous Media* (New York: Pergamon)
[3] Otto A 1965 *Z. Phys.* **185** 232
[4] Kloos T 1968 *Z. Phys.* **208** 77
[5] Ritchie R H 1957 *Phys. Rev.* **106** 874–81
[6] Kröger E 1968 *Z. Phys.* **227** 453
[7] Kröger E 1970 *Z. Phys.* **235** 403
[8] Howie A 1983 *Ultramicroscopy* **11** 141
[9] Garcia-Molina R, Gras-Marti A, Howie A and Ritchie R H 1985 *J. Phys. C: Solid State Phys.* **18** 5335–45
[10] Walls M G and Howie A 1989 *Ultramicroscopy* **28** 40–42
[11] Parker A 1988 Part 2 project, University of Cambridge
[12] Walsh C A 1991 Private communication
[13] Chen M and Bolton J P R 1992 *Superlatt. Microstruct.* **12** 531–4
[14] Chase J B and Kliewer K L 1970 *Phys. Rev.* B **2** 4389–400
[15] Bolton J P R and Chen M 1994 Dispersion brackets and electron energy loss *Open University Technical report*
[16] Stratton J S 1941 *Electromagnetic Theory* (New York: McGraw-Hill)
[17] Richter H and Geiger J 1981 *Z. Phys.* B **42** 39–45
[18] Chen M 1994 Applications of computer algebra to the theory of electron energy loss *PhD Thesis* Open University
[19] Ritchie R H and Eldridge H B 1962 *Phys. Rev.* **126** 1935–47
[20] Bolton J P R and Chen M 1995 *Ultramicroscopy* submitted
[21] Economou E N 1969 *Phys. Rev.* B **182** 539–54
[22] Pines D and Bohm D 1952 *Phys. Rev.* **85** 338–53
[23] Bolton J P R and Chen M 1995 *Ultramicroscopy* at press
[24] Feibelman P J 1982 *Prog. Surf. Sci.* **12** 287–407
[25] Lannoo M 1980 Surfaces and Interfaces *Electronic Structure of Crystal Defects and of Disordered Solids* ed F Gautier *et al* (Paris: Les Editions de Physique) pp 45–92